# Simulation-based optimization of the hydrofoil of a flying catamaran

Gianluca Meneghello<sup>1</sup>, Pooriya Beyhaghi, Thomas Bewley

UCSD Flow Control Lab

9500 Gilman Dr., 92093, La Jolla, CA

## 6 Abstract

A global optimization algorithm recently developed by our group, dubbed  $\Delta$ -DOGS, is applied to optimize the design of a racing catamaran's hydrofoil. A computationally inexpensive vortex-lattice based model of the hydrofoil, implemented in AVL (the Athena Vortex Lattice code), is used to compute the flow around the hydrofoil; the suitability of this inexpensive model for such a design optimization is considered carefully in light of available experimental data. While keeping the lift and side force of the hydrofoil constant, the optimization algorithm reduces the drag of the hydrofoil by over a factor of two.

- 7 Keywords: global optimization, derivative-free optimization, hydrofoil, vortex
- 8 lattice

#### 9 1. Introduction

- Hydrofoils play an increasingly important role in the design of high-performance
- sailboats and catamarans. The 34th America's Cup (San Francisco, 2013) high-
- 12 lighted the importance of efficient hydrofoil design, and the Class Rule for the
- 35th America's Cup (Bermuda, 2017), to be held on 48-foot catamarans, even
- <sup>14</sup> further emphasizes their importance: as hydrofoil design is now one of the few
- 15 features of the sailboat design left open in the competition rules. Hydrofoils
- 16 also play an increasingly important role on many sailboats outside of high-
- profile America's Cup races, including the Hydroptere (a large, fast trimaran),
- the International Moth class of small, fast sailing hydrofoils, and foil boards,

which are now quite popular for high-speed kiteboarding.

Accurate hydrofoil performance assessment and design optimization is, in general, a time-consuming and computationally expensive undertaking. Chal-21 lenges are present in both the physical and the numerical modeling: complex physics including boundary layers, free-surface effects, and cavitation generally 23 require high-fidelity numerical codes and large computational resources to assure 24 accurate results. Direct Numerical Simulations (DNS), Large Eddy Simulations (LES), and Reynolds-Averaged Navier-Stokes (RANS) simulations, however, are often unaffordable in the design phase, which often requires a significant 27 number of design iterations. Approximate performance estimates derived from computationally inexpensive models, such as vortex-lattice methods, are gen-29 erally sufficient for tuning the handful of adjustable parameters characterizing such designs. Numerical models of this sort are already well developed and used extensively for the design of rigid wings [11], and are applied here for the related problem of hydrofoil optimization. 33

The choice of the optimization algorithm for numerical design problems of 34 this level of complexity is as important as the choice of the physical model itself. Important trade-offs are present between computational cost and implementation complexity, as well as between the competing objectives of global explo-37 ration and local refinement in the design space. Derivative-free methods often have lower implementation complexity but higher computational cost, whereas 39 derivative-based methods often have have higher implementation complexity, as local derivative information must be computed, but lower computational cost. The competition between exploitation of local trends near existing datapoints, resulting in the determination of locally-optimal solutions, and the broader ex-43 ploration of the feasible domain, in search of globally-optimal solutions, must 44 be considered carefully.

Optimization methods designed to assure global convergence are usually derivative-free<sup>2</sup>. Such methods are often expensive in terms of the number

<sup>&</sup>lt;sup>2</sup>Note that some derivative-free methods in fact only assure local convergence, such as

of iterations required to converge, and generally scale rather poorly with the number of adjustable parameters to be optimized. The Surrogate Management Framework (SMF) developed in [6], and the Genetic Algorithms (GA) reviewed in [14], are examples of methods in this class. Applications of such methods in propeller and turbines' hydrofoil optimization are presented in [17] and [20].

Optimization methods designed to scale better to problems with a larger number of adjustable parameters, but which often only assure local convergence, are usually derivative-based, and use adjoint- or variational-based analyses to determine the gradient of the cost function and the constraints on the feasible domain with respect to the adjustable parameters, as reviewed in [15]. Such methods significantly reduce the number of iterations required to converge, though they can stall when gradients are approximated with finite differences based on inaccurate function evaluations [10]. Applications of such methods to propeller blade optimization include [13].

No broadly-available optimization methods today (derivative-based or derivative-62 free) rigorously handle uncertainty in the evaluation of the objective function 63 itself, automatically refining the function evaluations as convergence is approached. Such uncertainty may be related, for example, to the mesh size used in the simulation, or to the time averaging of the lift and drag in an unsteady simulation or experiment. Derivative-free approaches are generally the 67 best available methods for such problems, as they tend to keep function evalua-68 tions far apart until convergence is approached, thereby minimizing the negative effects of uncertainty in the function evaluations. Our team is in the process of developing a powerful new method, which automatically refines the function 71 evaluations as convergence is approached, for problems of this important class; 72 the reader is referred to [3] for details. 73

In this work, we consider the application of our new derivative-free optimization algorithm dubbed  $\Delta$ -DOGS (developed in [5]) to the design of a 3D hydrofoil with seven adjustable parameters. The computationally inexpensive

<sup>[2, 16].</sup> 

vortex-lattice model implemented in AVL (the Athena Vortex Lattice code; see [8]) is used to compute the lift and drag coefficients of the hydrofoil.

This paper is organized as follows. In  $\S 2$ , we describe the AVL model, discuss its limitations, and presents a careful validation based on experimental results from the literature. Next,  $\S 3$  describes the parametrization of the hydrofoil used in the present optimization, and the reasoning behind the particular choice of parameters used. In  $\S 4$ , we briefly review the new global optimization algorithm applied to the problem,  $\Delta$ -DOGS. The results of our optimization study are presented in  $\S 5$ , and conclusions are drawn in  $\S 6$ .

#### 86 2. Hydrofoil model and validation

The numerical model used to compute the function evaluations in this work,
AVL [8], determines the inviscid lift and drag coefficients of the hydrofoil based
on a vortex-lattice discretization, as illustrated in Figure 1; see [12] for a detailed
description of this classic technique. The viscous drag is approximated based
on the local lift coefficient  $C_L$  from the foil sections'  $C_D$  ( $C_L$ ) curve, where  $C_D$ is the drag coefficient [1].

AVL implements a "free-surface" boundary condition in the form of a constantpressure, constant-height horizontal plane. This is known to be a good approximation of a true free surface in the limit of high Froude numbers [9, chapt. 6],

correctly modeling the inviscid lift and drag. However, this approximation is unable to capture other effects associated with the presence of a free surface, such as wave drag, the relative importance of which grows at lower Froude numbers, and cavitation, appearing at higher Froude numbers. It is thus informative to compare AVL-based predictions with available experimental data in representative configurations. For this purpose, we consider water-tank measurements of a rectangular hydrofoil with an aspect ratio of 10 and a NACA64<sub>1</sub>-412 foil section, as reported in [18].

Table 1 presents numerical results, computed with AVL, and experimental measurements for the  $dC_L/d\alpha$  coefficient ( $\alpha$  being the angle of attack in degrees),

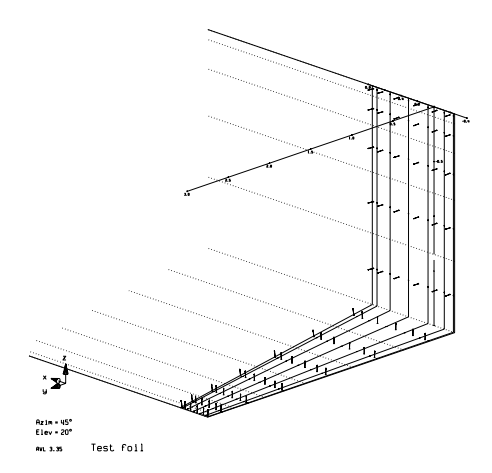


Figure 1: The vortex lattice model: the foil is discretized by vortices which are distributed in the spanwise direction along the foil, and extended to infinity past the edge of the foil (dotted lines). The intensity of these vortices are then obtained by imposing zero velocity across the foil surface at the points marked by the small arrows. Lift and inviscid drag can then be computed as a function of the intensity of the vortices.

Table 1: Comparison between AVL and experimental results

		$\mathrm{AVL}^a$	$\operatorname{Exp}^b$	$\mathrm{Err}^c$	$\%\mathrm{Err}^d$
depth = 0.84c	$dC_L/d\alpha$	0.071	0.071	0.000	0.0%
$(Fn_{\dot{h}}=10.48)$	$\alpha(C_L=0)$	-3.28	-3.3	0.0	0.6%
	$C_D(C_L = 0.4)$	0.01378	0.016	-0.002	13.9%
	$C_D(C_L = 0.6)$	0.02476	0.028	-0.003	11.6%
depth = 3.84c	$dC_L/d\alpha$	0.0817	0.083	-0.001	1.6%
$(Fn_h=4.97)$	$\alpha(C_L=0)$	-3.15	-3.2	0.1	1.6%
	$C_D(C_L = 0.4)$	0.01167	0.014	-0.002	16.6%
	$C_D(C_L = 0.6)$	0.01981	0.022	-0.002	10.6%

Only significant digits are reported in each entry.

<sup>&</sup>lt;sup>a</sup> AVL result, viscous coefficients obtained from [1]

<sup>&</sup>lt;sup>b</sup> Data from [18], values are for the highest speed tested in the deepest tank

 $<sup>^{</sup>c}\,\mathrm{AVL}-\mathrm{Exp}$ 

 $d \left\| \frac{\text{AVL-Exp}}{\text{Exp}} \right\|$ 

the angle of attack for zero lift  $\alpha(C_L=0)$ , and the total drag coefficient  $C_D$  at two different lift conditions,  $C_L=0.4$  and  $C_L=0.6$ . Two different depths of submergence are tested,  $h=0.84\,c$  and  $h=3.84\,c$ , where c is the hydrofoil chord. The submergence depth h is defined as the distance between the undisturbed free surface and the quarter-chord location of the foil. The two configurations considered correspond to depth-based Froude numbers of  $Fn_h=\frac{U}{\sqrt{g\,h}}=10.48$  and 4.97, respectively.

The AVL results for  $dC_L/d\alpha$  in Table 1 are obtained via a least-square fit of a straight line through the  $C_L(\alpha)$  data computed over the range  $-3.5 < \alpha < 6.0$ . Drag results are obtained by running the AVL model with the desired lift as a constraint. The viscous drag is obtained from the wind-tunnel measurements reported in [1].

Experimental data is obtained from Figures 10 and 11 of [18]; only results for the largest water tank and the highest speed considered, equivalent to a chord-based Froude number of  $Fn_c = U/\sqrt{gc} \approx 10$ , are used. All significant digits that can be reliably obtained by digitalization of the figures in [18] are reported.

It is seen that the agreement between the numerical (AVL) and the avail-123 able experimental data for the hydrofoil lift is exceptionally good, with an error 124 everywhere less than 2% for both depths tested. The agreement for the hydro-125 foil drag, however, appears to be diminished, with the AVL model consistently 126 underestimating the experimental drag by  $\Delta C_D \approx 0.002$ , or by 10 - 15%. Dis-127 crepancies in the drag coefficient data should be considered with care, however; 128 the difference between numerical and experimental results, at 0.002, is well 129 within the range of variation due to the free-stream turbulence intensity (see 130 Figure 5. Its independence of depth suggests that such a discrepancy is not 131 related to the lack of wave drag modeling in AVL, as wave drag is expected to 132 depend strongly on depth. Rather, we suggest three alternative explanations: 133

• differences in the experimental Reynolds number between [18] ( $Re = 1.5 \times 10^6$ ) and [1] ( $Re = 3.0 \times 10^6$ ),

134

135

- differences in the free stream turbulence levels in the water-tank measurements of [18] and the wind tunnel measurements of [1], causing a different boundary layer transition location, and/or
- the possibly neglected effects associated to the strut-hydrofoil interaction in the experimental data that is, the total drag of the strut-hydrofoil combination was first measured, then the drag of the strut alone was subtracted off.

Regardless of the reason for the discrepancies in the drag coefficient, it is seen in Table 1 that the AVL model correctly captures the *lift* properties of the foil at both tested depths, and correctly captures the *changes in drag* associated with changes in the lift coefficient and depth. For the purpose of this work, we thus consider the AVL model to be well suited. Further comparisons with experimental results, as well as numerical simulations with more accurate codes, should be pursued in future work.

## 3. Parametrization of the hydrofoil

160

161

162

Due to their computational cost, global optimization algorithms are generally quite limited in the number of tunable parameters that can be effectively optimized. The parametrization of the geometry is thus a very important step of the optimization process when using such algorithms.

The hydrofoil parametrization used in the present work is visualized in Figure 2. The reference system used has z as the vertical (positive up) coordinate, y as the horizontal crossflow coordinate, and x as the horizontal streamwise coordinate. A curvilinear coordinate s is also defined along the quarter-chord of the foil, with its origin at the free surface.

A key parameter defining the hydrofoil is the planform surface area S. A minimum surface area, representing a lower bound for the parameter S during the optimization process, is prescribed in order to assure a physically realizable airfoil. The optimization process then balances the contribution of the viscous

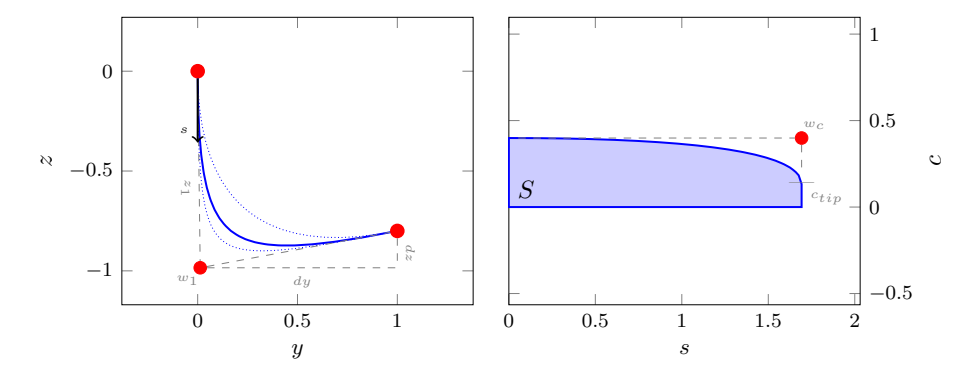


Figure 2: Parametrization of the shape of the hydrofoil, which is defined by seven parameters describing two rational Bezier curves. (left) Front view of the y-z plane. The shape of the quarter-chord line in this plane is defined by  $z_1$ , dy, and dz, together with the weight  $w_1$ . Dotted lines show the effect of changing the weight  $w_1$  on the shape of the foil. (right) Planform view. The spanwise distribution of the chord length in this plane is defined by the planform area S, together with the tip chord length  $c_{tip}$  and the weight  $w_c$ .

drag, proportional to the surface area S, and the inviscid drag, proportional to the square of the lift coefficient (equivalently, to the inverse of the surface area).

The other parameters illustrated in Figure 2 define the hydrofoil shape in the y-z plane and the chord distribution along the curvilinear coordinate s.

Both the shape of the hydrofoil's quarter-chord line as well as the shape of the hydrofoil's trailing edge are represented using Bezier curves defined by

$$\mathbf{x}(t) = \frac{\sum_{i=0}^{n} b_{i,n} \mathbf{P}_{i} w_{i}}{\sum_{i=0}^{n} b_{i,n} w_{i}}, \qquad b_{i,n} = \binom{n}{i} t^{i} (1-t)^{n-i},$$
(1)

where  $\boldsymbol{x}=(y,z), \, \boldsymbol{P}_i=(y_i,z_i)$  are the control points marked in red in Figure 2, and  $w_i$  are the weights of the control points.

The relative importance of the parameters on the foil efficiency is presented

## 4. Optimization Algorithm

in Figure 3.

173

175

176

177

In this section, we introduce the  $\Delta$ -DOGS algorithm used to optimize the hydrofoil design. As described in [4, 5],  $\Delta$ -DOGS is an efficient, globally-convergent, derivative-free optimization algorithm designed to solve general optimization problems of the form

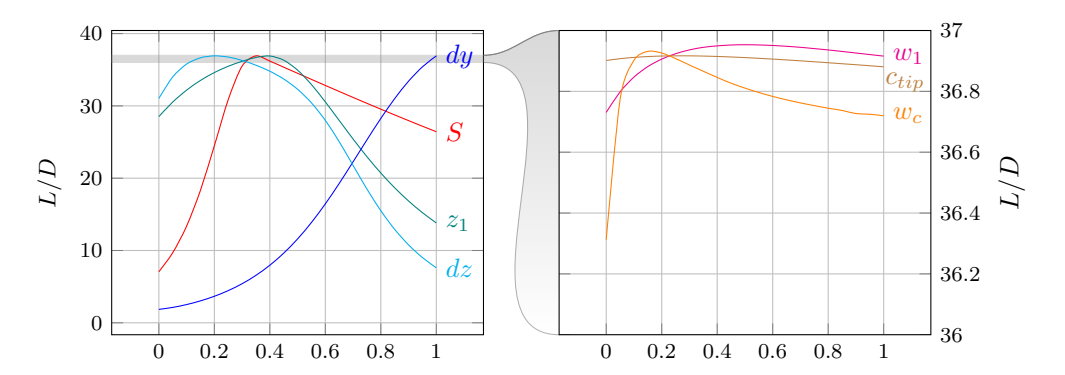


Figure 3: Variation of the hydrofoil efficiency as a function of the parameters, normalized to lie between 0 and 1. To produce these plots, each parameter is varied, one at a time, between 0 and 1, while the other parameters are held fixed at their optimum values, for the case with  $dy \leq 1.50$  (see Table 3). Left: S,  $z_1$ , dy, and dz each contribute strongly to the variation in efficiency. Right:  $w_1$ ,  $c_{tip}$ , and  $w_c$  each contribute only weakly to the variation in efficiency (note the rescaled vertical axis).

minimize 
$$f(x)$$
 subject to  $Ax \le b$  (2)

The algorithm is initialized with n+1 affinely independent points in the feasible 179 domain  $Ax \leq b$ , where x is the vector of adjustable parameters and n is the order of x. These feasible n+1 points are selected such that they generate a 181 simplex with the maximum possible volume within the feasible domain (see [4]). 182 After this initialization, each successive iteration k of the algorithm performs 183 a single function evaluation, and updates a "surrogate" model of the objective 184 function f(x). This model consists of an interpolation p(x) of the function values currently available, as well as an associated model of the uncertainty of 186 this surrogate, e(x). In the present work, we assume that an estimate  $f_0$  of the 187 value of the global minimum  $f(x^*)$  is available, where  $x^*$  is the location of the 188 optimum in parameter space, which we desire to find. Based on the surrogate 189 model, a feasible point  $x_k$  is identified at each iteration k which, within this 190 model, has the highest probability of attaining the value of  $f_0$ . Particular care 191 is taken in the vicinity of the boundary: if the point  $x_k$  is sufficiently close to the 192 boundary of the convex hull of the existing data points, it is projected out to the 193 boundary of the feasible domain; this feasible boundary projection procedure

is described in detail in §3 of [4]. In the present work, as in [4, 5], we have used polyharmonic spline interpolation [19] for the interpolation strategy, and 196 the uncertainty function e(x) is defined as a piecewise quadratic function built 197 on the framework of a Delaunay triangulation  $\Delta^k$  of the existing datapoints in 198 parameter space. 199

The essential steps of the  $\Delta$ -DOGS algorithm used in this work are outlined in Algorithm 1 and illustrated in 4; complete description of this algorithm, as well as proof of its convergence, may be found in [4].

The performance of  $\Delta$ -DOGS depends on two main parameters:

200

201

202

203

204

205

206

207

208

209

210

211

212

213

214

215

216

217

218

- $f_0$ , an estimate of the bound for the optimal value  $f(x^*)$ . If  $f_0 \leq f(x^*)$ , convergence to the global minimum is guaranteed; however, if  $f_0$  is significantly smaller than  $f(x^*)$ , the speed of convergence is substantially reduced. If  $f_0 > f(x^*)$  the algorithm terminates at a feasible point z such that  $f(z) < f_0$ , and convergence to the global minimum is not guaranteed.
- $\bullet$   $\delta_0$ , the minimum allowed distance in parameter space between the current search point  $x_k$  and the previously evaluated points  $x \in S^k$ ;  $\delta_0$  is used to set a termination condition for the algorithm.

To set up the present optimization problem, bounds for all seven of the tunable parameters must be selected to specify the feasible domain of the search,  $\delta_0$ must be selected to define the stopping criterion, and, perhaps most importantly, an estimate of a bound for the objective function value,  $f_0 = \max(L/D) =$  $\max(C_L/C_D)$ , must be identified.

The objective function bound,  $f_0$ , can be obtained using classical aerodynamic theory. The drag coefficient for an aspect ratio AR and elliptic spanwise load is: 219

$$C_D = \frac{C_L^2}{\pi AR} + C_{D\nu} \left( C_L \right), \tag{4}$$

where  $C_{D\nu}(C_L)$  is the drag coefficient for the two dimensional foil section and can be obtained from experimental data [1] or computationally inexpensive nu-

## Algorithm 1 Δ-DOGS: minimize $f(x) : \mathbb{R}^n \to \mathbb{R}$ subject to $Ax \leq b$ .

- 1: Set k = 0. Determine the set  $S^0$  of n + 1 points in the feasible domain that form the vertices of a simplex with the maximum possible volume (see §2 of [4]). Calculate f(x) at all points  $x \in S^0$ .
- 2: Calculate (or, for k > 0, update) an appropriate interpolating function  $p^k(x)$  through all points in  $S^k$ .
- 3: Calculate (or, for k > 0, update) a Delaunay triangulation  $\Delta^k$  over all of the points in  $S^k$ .
- 4: Find  $x_k$  as a global minimizer of  $s^k(x)$  to obtain  $x_k$ , where

$$s^{k}(x) = \begin{cases} \frac{p^{k}(x) - f_{0}}{e^{k}(x)}, & \text{if } p^{k}(x) \ge f_{0}, \\ p^{k}(x) - f_{0}, & \text{otherwise,} \end{cases}$$
 (3)

where  $e^{k}(x)$  is the uncertainty function for the datasset  $S^{k}$ .

- 5: If  $x_k$  is sufficiently close to the boundary of the convex hull of the available datapoints, project  $x_k$  out to the boundary of feasibility (see §3 of [4]).
- 6: Set  $\delta = \min_{x \in S} ||x_k x||$ . If  $\delta > \delta_0$  (see [4]), set  $S^{k+1} = S^k \cup \{x_k\}$ , evaluate  $f(x_k)$ , and repeat from 2; otherwise, stop.

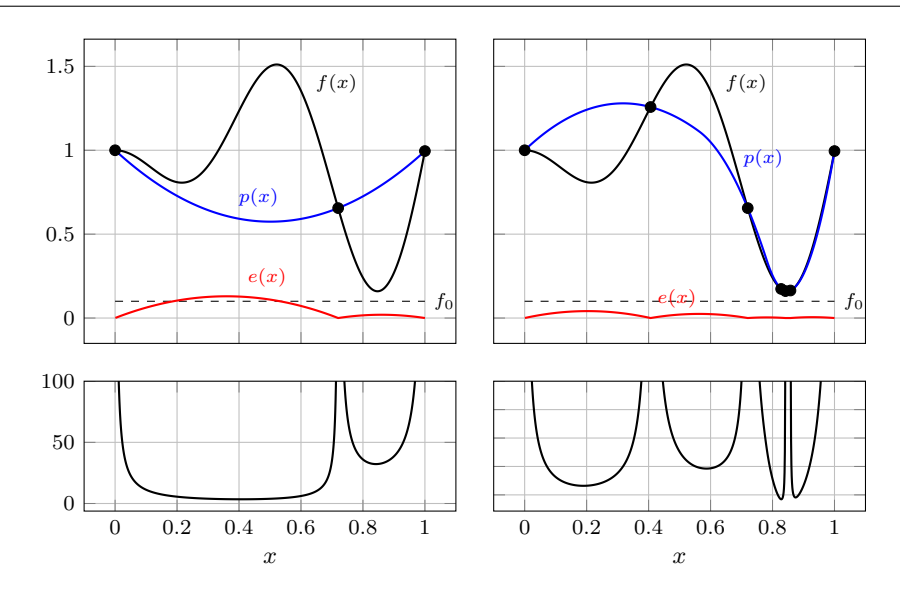


Figure 4: Illustration of the  $\Delta$ -DOGS optimization algorithm for a one-dimensional example. Left column: status of optimization after three function evaluations have been performed. Right column: status after the optimization algorithm has terminated. Top row: (black) objective function f(x), (blue) interpolation p(x), (red) uncertainty e(x), and (dashed) estimate of the global minumum  $f_0$ . The function values available to the optimization algorithm are marked as black circles. Bottom row: the search function  $s(x) = (p(x) - f_0)/e(x)$ .

merical models [7]. Figure 5 shows drag coefficients for the NACA64<sub>1</sub>-412 foil 222 section (left), and efficiency curves for an aspect ratio 10 foil with elliptic load 223 based on (4) (right). No free-surface effects are taken into account. Curves 224 are shown for two different values of the boundary layer transition parameter, 225  $n_c = 4$  and  $n_c = 9$ , as well as for a fully turbulent boundary layer. Both the 226 maximum achievable efficiency and the corresponding optimal lift coefficient  $C_L$ 227 depend strongly on the transition location of the boundary layer. In the rest of 228 this work, the same NACA64<sub>1</sub>-412 will be used for the case with  $n_c = 4$ . At 229 AR = 10, the corresponding estimated bound for the efficiency is  $f_0 = 38$ . 230

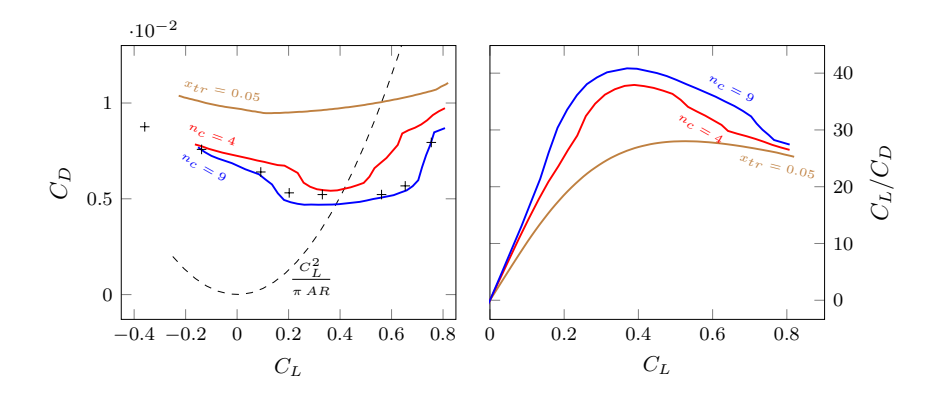


Figure 5: NACA64<sub>1</sub>-412 wing section polar curves (left) and efficiencies for AR=10 (right) for two values of the boundary layer transition parameter, (blue)  $n_c = 9$ , (red)  $n_c = 9$ , as well as (brown) an almost completely turbulent boundary layer. Viscous drag coefficients are computed with XFoil [7]. Experimental drag coefficients from [1] are marked with +.

#### 5. Optimization results

The optimization of the L/D ratio for the surface lifting foil described by the parametrization in Figure 2 is performed for a design vertical and horizontal lift  $SC_z = 0.120$  and  $SC_y = 0.066$ , with bounds on the parameters as given in Table 2. The vortex lattice method implemented in AVL is used to compute lift and inviscid drag, with the free surface modeled as a horizontal constant pressure surface. The viscous drag coefficient is obtained by interpolation of

Table 2: Bounds on the hydrofoil parametrization.

$$0.2 \le S \le 0.5$$
 
$$0.5 \le z_1 \le 1.5 \qquad 0.5 \le dy \le 1.5 \qquad -0.3 \le dz \le 0.3 \qquad 4.3 \le w_1 \le 11$$
 
$$0.05 \le c_{tip} \le 0.5 \qquad 1.5 \le w_c \le 11$$

experimental wind-tunnel data [1]. Validation of the model is provided in §2. 238 The convergence history for the optimization process is shown in Figure 6. 239 An L/D of 32 is obtained after only 23 function evaluations; approximately 160 240 function evaluations are needed to reach the maximum L/D of 36.81. Given 24: that this is a seven-dimensional optimization problem, with four of the param-242 eters turning out to strongly affect the objective function (see Figure 3), the 243 performance of our derivative-free optimization algorithm,  $\Delta$ -DOGS, on this 244 practical optimization problem is deemed quite satisfactory. A gradient based 245 optimization requires, on average and depending on the initial guess, a similar 246 number of function evaluation if the gradient is computed by finite difference. Figure 7 indicates the optimal geometry identified by the optimization al-248 gorithm, as well as the ensemble of other geometries tested. The optimized 249 parameters are reported in Table 3. It is noted that, at the optimized condi-250 tion, only dy is at one of its bounds; the other six optimized parameters are 251 on the interior of the feasible domain. The optimized results for two different upper bounds on dy are indictated in the two columns of Table 3. 253

## 6. Conclusions

A global optimization algorithm recently introduced by our group,  $\Delta$ -DOGS, has been applied to optimize the design of a flying-catamaran hydrofoil, with the goal of maximizing the lift/drag ratio at a specified working condition. The vortex-lattice model implemented in AVL has been used to compute the hydrofoil's lift and drag characteristics. The AVL model has been validated for this problem with experimental data available in the literature.

Table 3: Optimal parameters for two different bounds for dy

parameter	$dy \le 1.50$	$dy \le 2.00$
S	0.305	0.305
$z_1$	0.89	1.30
dy	1.50	2.00
dz	-0.29	-0.27
$w_1$	7.25	4.33
$c_{tip}$	0.21	0.43
$w_c$	2.58	3.60
$\frac{L}{D}$	36.81	47.60
$\alpha$	3.78699	3.29558
β	0.02691	-0.07407

While a first-guess, L-shaped, constant chord design with  $z_1 = dy = 1.5$ 261 and a surface area S=0.3050 has an  $L/D\approx 15$ , the optimized hydrofoil has 262 an  $L/D \approx 35$ , which represents a 2.3× improvement. This work thus shows 263 how computationally inexpensive numerical models can be successfully coupled 264 with efficient global optimization algorithms on nontrivial practical problems, providing valuable design guidance for the early stages of the design process. 266 We conclude by noting that the model implemented in AVL is valid only 267 for chord-based Froude numbers  $Fn_c \approx O(10)$ . Below that, unmodeled wave 268 generation becomes significant [9, section 6.8], while above that phenomena like 269 cavitation or ventilation kick in. As a point of comparison, the hydrofoil of 270 an AC72 boat, having a 0.7m chord and sailing at 40 knots (20m/s), has an 271  $Fn_c = \frac{20}{\sqrt{9.81 \cdot 0.7}} = 7.63$ . The efficient use of more computationally intensive, high-fidelity numerical codes for optimization, able to correctly capture a larger 273 range of Froude numbers, will be investigated in future work.

## 75 Acknowledgements

The authors gratefully acknowledge seed funding from Leidos in support of this effort.

278

- [1] Ira Herbert Abbott and Albert Edward Von Doenhoff. *Theory of wing*sections, including a summary of airfoil data. Courier Corporation, 1959.
- <sup>281</sup> [2] Charles Audet and John E Dennis Jr. Mesh adaptive direct search algorithms for constrained optimization. SIAM Journal on optimization, 17(1):188–217, 2006.
- <sup>284</sup> [3] Pooriya Beyhaghi and Thomas Bewley. Delaunay-based derivative-free optimization for efficiently minimizing infinite time-averaged statistics. *Jour-*<sup>286</sup> nal of Global Optimization, 2016. under review.
- <sup>287</sup> [4] Pooriya Beyhaghi and Thomas Bewley. Delaunay-based derivative-free op-<sup>288</sup> timization via global surrogates, part II: Convex constraints. *Journal of* <sup>289</sup> *Global Optimization*, 2016.
- [5] Pooriya Beyhaghi, Daniele Cavaglieri, and Thomas Bewley. Delaunay based derivative-free optimization via global surrogates, part I: linear constraints. Journal of Global Optimization, pages 1–52, 2015.
- <sup>293</sup> [6] Andrew J Booker, JE Dennis Jr, Paul D Frank, David B Serafini, Virginia Torczon, and Michael W Trosset. A rigorous framework for optimization of expensive functions by surrogates. *Structural optimization*, 17(1):1–13, 1999.
- [7] Mark Drela and Michael B Giles. Viscous-inviscid analysis of transonic and
   low reynolds number airfoils. AIAA journal, 25(10):1347–1355, 1987.
- [8] Mark Drela and Harold Youngren. AVL Athena Vortex Lattice. http://web.mit.edu/drela/Public/web/avl/. [Online; accessed 26-August-2015].

- [9] Odd M Faltinsen. *Hydrodynamics of high-speed marine vehicles*. Cambridge university press, 2005.
- [10] Philip E Gill, Walter Murray, and Michael A Saunders. Snopt: An sqp
   algorithm for large-scale constrained optimization. SIAM review, 47(1):99–
   131, 2005.
- [11] K Graf, Av Hoeve, and S Watin. Comparison of full 3d-rans simulations
  with 2d-rans/lifting line method calculations for the flow analysis of rigid
  wings for high performance multihulls. Ocean Engineering, 90:49–61, 2014.
- [12] Joseph Katz and Allen Plotkin. Low-speed aerodynamics, volume 13. Cambridge University Press, 2001.
- [13] Kyung-Jun Lee, Tetsuji Hoshino, and Jeung-Hoon Lee. A lifting surface optimization method for the design of marine propeller blades. *Ocean Engineering*, 88:472–479, 2014.
- <sup>315</sup> [14] Melanie Mitchell. An introduction to genetic algorithms. MIT press, 1998.
- [15] Jorge Nocedal and Stephen Wright. Numerical optimization. Springer
   Science & Business Media, 2006.
- <sup>318</sup> [16] Virginia Torczon. On the convergence of pattern search algorithms. SIAM

  Journal on optimization, 7(1):1–25, 1997.
- [17] Florian Vesting and Rickard E Bensow. On surrogate methods in propeller optimisation. *Ocean Engineering*, 88:214–227, 2014.
- [18] Kenneth L Wadlin, Charles L Shuford, and John R McGehee. A theoretical and experimental investigation of the lift and drag characteristics of hydrofoils at subcritical and supercritical speeds. Technical report, Langley
  Aeronautical Laboratory, Langley Field, Va, 1955.
- <sup>326</sup> [19] Grace Wahba. Spline models for observational data, volume 59. Siam, 1990.

[20] B Yang and XW Shu. Hydrofoil optimization and experimental validation
 in helical vertical axis turbine for power generation from marine current.
 Ocean Engineering, 42:35–46, 2012.

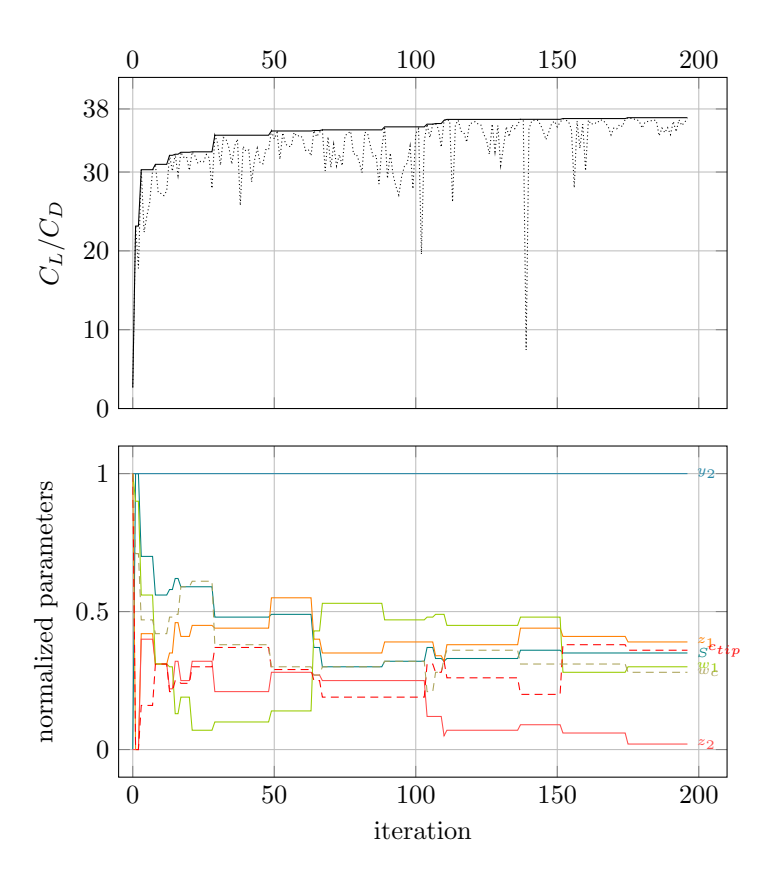


Figure 6: Convergence history. Top: best efficiency  $C_L/C_D$  (solid) at constant lift during the optimization; the actual value at each iteration is showed by a dotted line. Bottom: optimal parameter's values during the optimization.

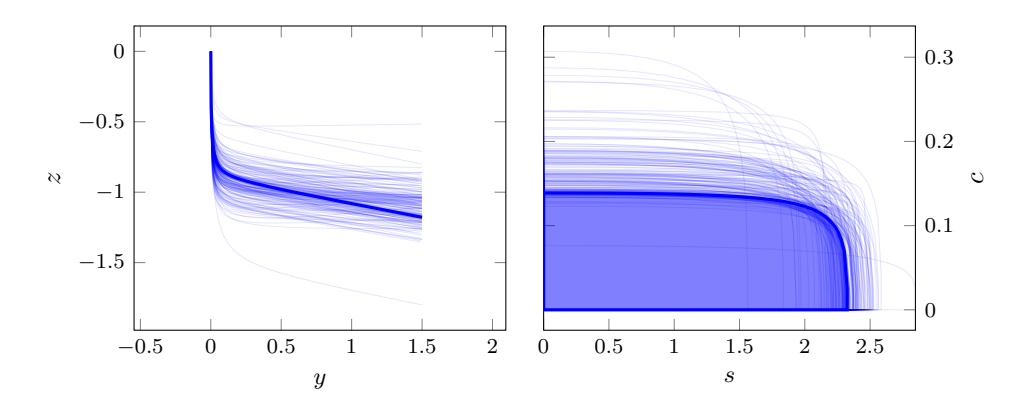


Figure 7: Optimized geometry (thick), and all tested geometries (thin).

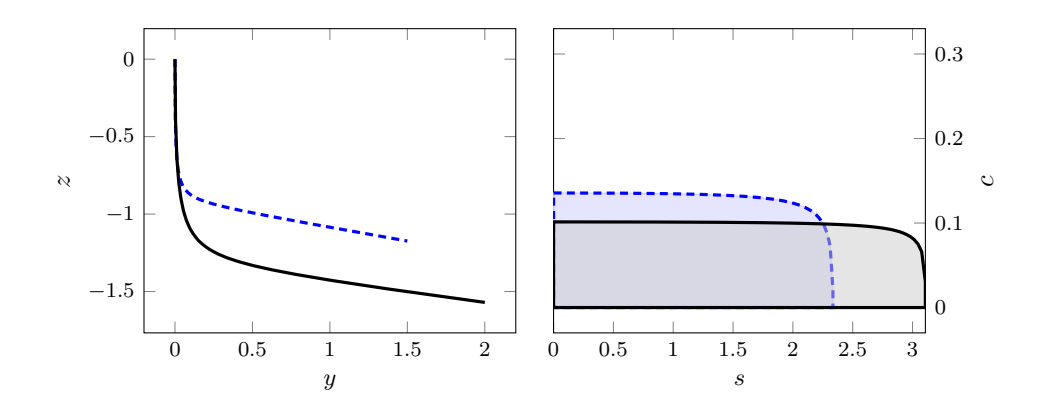


Figure 8: Optimized geometries with two different aspect ratios.